Chapter 1

Introduction and Literature Survey

1.1 Global warming and energy security

Energy security due to depletion of fossil fuels and Global warming due to net carbon increase in earth's atmosphere to continuous burning of fossil fuels to fulfil our energy needs are two major challenges the world is facing today. Thus global warming and energy security are major concerns that feature routinely in public policy discourses around the world.

1.1.1 Global warming and Climate change

1.1.1.1 Global warming

Global warming is the phenomenon that measures the increase in average air temperatures near the surface of Earth over the past one to two centuries. Scientists have observed various weather phenomena (such as temperatures, precipitation, and storms) and related influences on climate (such as ocean currents and the atmosphere's chemical composition. [1-2] Primarily fossil fuel burning, human activities, and Industrial Revolution continuously increase the heat-trapping greenhouse gas levels in Earth's atmosphere that influence climate change. The Inter-governmental Panels on Climate Change (IPCC) and the United Nations Framework Convention on Climate Change (UNFCCC) have identified climate change as the greatest threat to human beings as the average temperature on earth has risen to 0.74^{o} C and increasing continuously. The concentration of carbon dioxide (CO_2) increases by 385 ppm (parts per million) which is far more than at any time in the last 650,000 years, participating majorly in climate change or global warming. [3-7]. **Figure 1.1** shows the distribution of temperature worldwide.

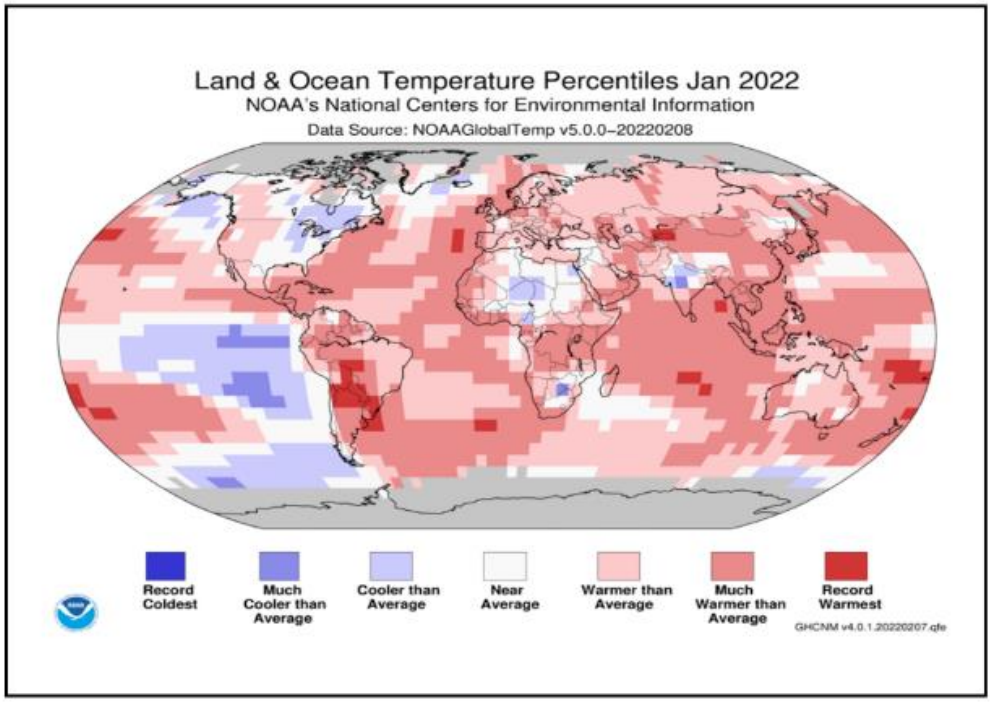

Figure 1.1 Illustration of Global Warming [1]. (Figure is taken from open access internet source)

1.1.1.2 causes of global warming and Climate change

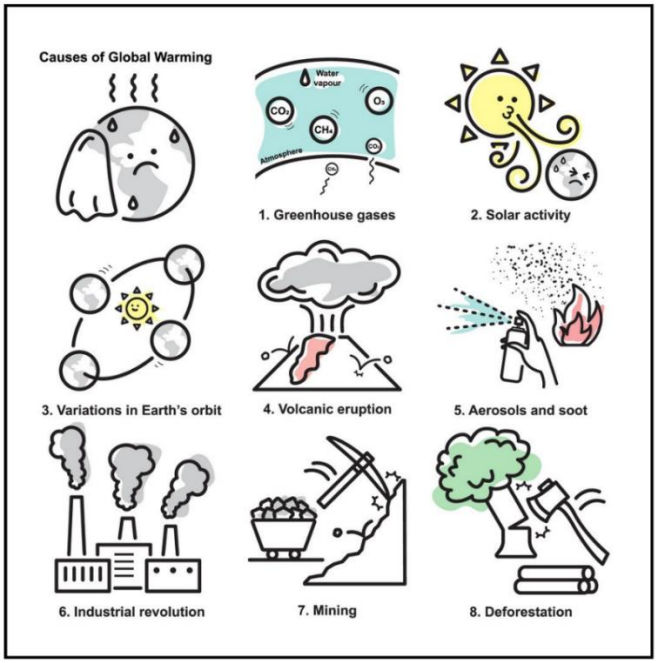

Figure 1.2. causes of global warming and Climate change [8]. (Figure is taken from open access internet source)

Climate change is a long-term shift of weather conditions that is identified by changes in temperature, precipitation, winds, and other indicators. Climate change can involve both changes in average conditions and changes in variability, including, for example, extreme events. The earth's climate is naturally variable on all time scales. However, its long-term state and average temperature are regulated by the balance between incoming and outgoing energy, which determines the Earth's energy balance. Any factor that causes a sustained change to the amount of incoming energy or the amount of outgoing energy that can lead to climate change is a long-term change in the average weather patterns that have come to define Earth's local, regional and global climates. [8-12]

1.1.1.3 Causes of climate change

1. Net Carbon dioxide and nitrous oxide edition in the earth`s environment that is produced by burning fossil fuels such as coal, oil, and natural gas.
2. Mining and cutting down forests (deforestation). Trees absorbed a lot of CO_2 during photosynthesis and maintain CO_2 levels and balance the atmosphere.
3. Fertilizers containing nitrogen produce nitrous oxide emissions during farming
4. Human activities and the Industrial revolution always increase greenhouse gas emissions in the atmosphere.

1.1. 2 Energy security

Energy security is a complex term and its implications happen in a wide range of spheres political, economic, environmental, social, technical, etc. The concept of energy security became interconnected with other environmental, social, political, and security issues due to climate change. Globalization and the uncertain future of fossil fuels give a new dimension, its parameter belongs to sustainability, energy efficiency, mitigation of greenhouse gas emissions, and accessibility of energy services.[13-17]

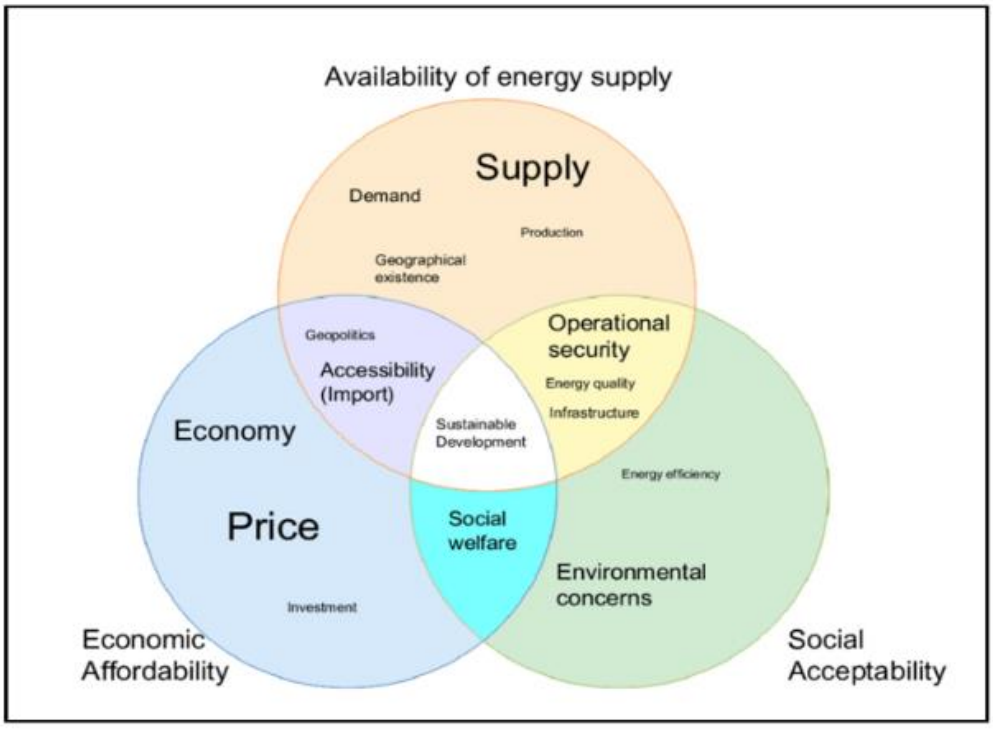

Figure 1.3. Concept of energy security[12]. (Figure is taken from open access internet source)

1.2 Pollution control and green energy over fossil fuel

Pollution is a by-product of unwanted harmful gases that are released during the burning of fossil fuels , indrustries and its spread into the air, nowadays increasing gradually but when contention of the pollutants rises to a certain limit, it is a threat to human beings and the environment. When fossil fuels are burned, they release CO_2, SO_2, nitrogen oxides, and unburnt hydrocarbons into the atmosphere, which contributes to the formation of smog and acid rain. The most common nitrogen-related compounds emitted into the air by human activities are collectively referred to as nitrogen oxides. Ammonia is another nitrogen compound emitted into the air, primarily from agricultural activities, but also from fossil fuels. Most of the nitrogen oxides released due to human activity are from the burning of fossil fuels associated with transportation and industry. [17-18]

1.3 Renewable energy and alternative energy solutions

Renewable energy is a sustainable energy solution for reducing the net carbon addition or CO_2 emissions and energy-related environmental problems. Now the world is fast becoming a global village due to the increasing daily requirement of energy for all populations across the world. Renewable energy has received noteworthy attention during the last few decades for new alternating energy sources. Renewable energy resources like geothermal energy, wind energy, hydropower, biomass, and solar energy have been considered to get to a more sustainable future.[19-21] **Figure 1.4(a-b)** shows the renewable energy sources and energy consumption of different sources.

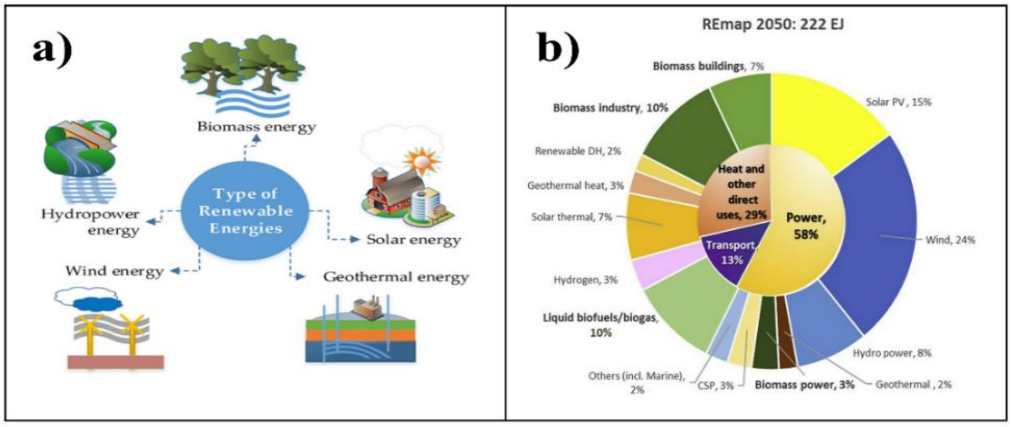

Figure 1. 4. a) Source of renewable energy [18] b) Breakdown of renewables use in total final energy consumption terms, REmap 2050 [19] (Figures are taken from open access internet source)

Table 1.1 Type of renewable energy source and application [21]

Source	**Energy conversion and usage options**
1. Hydropower	Power generation from flowing water
2. Biomass	Heat and power generation, pyrolysis, gasification, digestion
3. Geothermal	Urban heating, power generation, hydrothermal, hot dry rock
4. Solar	Solar home systems, solar dryers, solar cookers, Photovoltaic, thermal power generation, water heaters
5. Wind Power	Power generation, wind generators, windmills, water pump

1.4 Limitation/ problem with Renewable energy

The source of Renewable energy has some limitations,

1. Power and current fluctuation

2. A time and weather depended on the energy supply

3. Not suitable to use directly in electrical appliances due to power fluctuations and production uncertainties.

That is why energy storage is key for smooth power regulation/delivery. Thus, to get as per demand uninterrupted fixed power and current, energy storage devices are a must.

1.5 Type of energy storage solutions

Energy storage gives a well-established approach to improving grid-scale reliability and utilization. Whereas transmission and distribution systems can be moved over distances to end-users. Generally, available Grid-scale energy applications storage technologies are

1. Mechanical, 2. Electric, 3. Chemical, and 4. Electrochemical.[22-26]

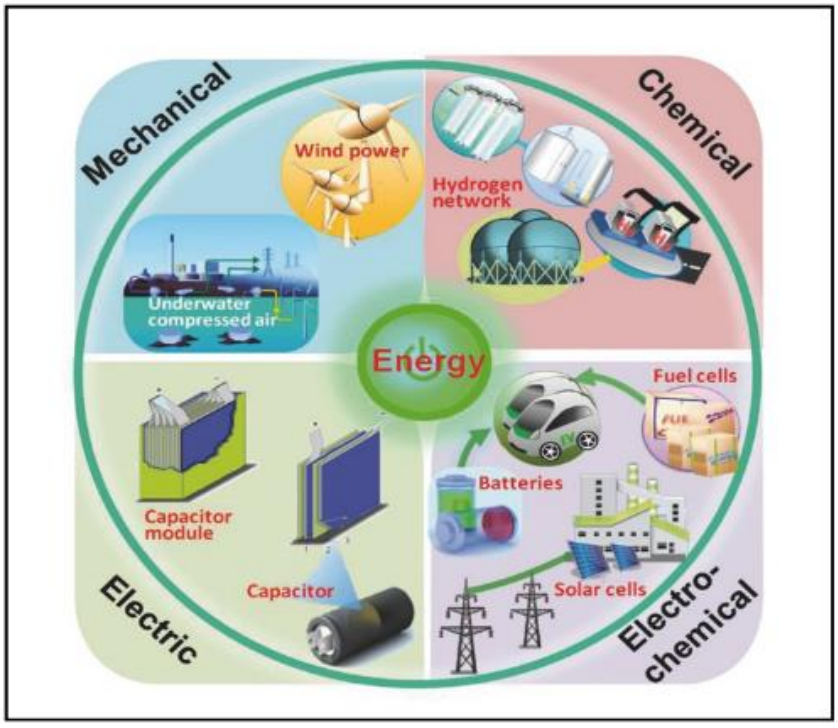

Figure 1.5 Different types of grid energy storage technologies for stationary applications [26]. (Figure is taken from open access internet source)

The electrochemical energy storage devices are an alternating energy storage solution to store renewable energy for high-value applications for energy storage ranging from the integration of renewable energy sources to power quality and reliability.[23] Hydroelectricity or mechanical energy storage via pumped is now a dominant energy storage method but electrochemical energy storage systems in terms of metal sulfur battery, metal-air (Li-air, Zn-air) battery, electrochemical capacitors (ECs,) and batteries hold great potential in the grid-sale applications due to its high conversion efficiency. Chemists and materials scientists now focus on cheap, sustainable, and recyclable materials having low manufacturing and maintenance costs, and long cycle life for electrochemical energy storage devices. Electrochemical energy storage devices store chemical energy through faradic (redox control) and non-faradaic (surface control like EDLC) processes. Electric double-layer capacitors (EDLCs) are suitable for power management (e.g., frequency regulation), but deliver a low energy density. Alternatively, redox control mode electrical energy can be stored as chemical energy by faradaic oxidization and reduction of the electrochemically active reagents that can deliver high energy density. [24-27] **Figure1.6** represent the Ragone plot of different type of energy storage devices. [27]

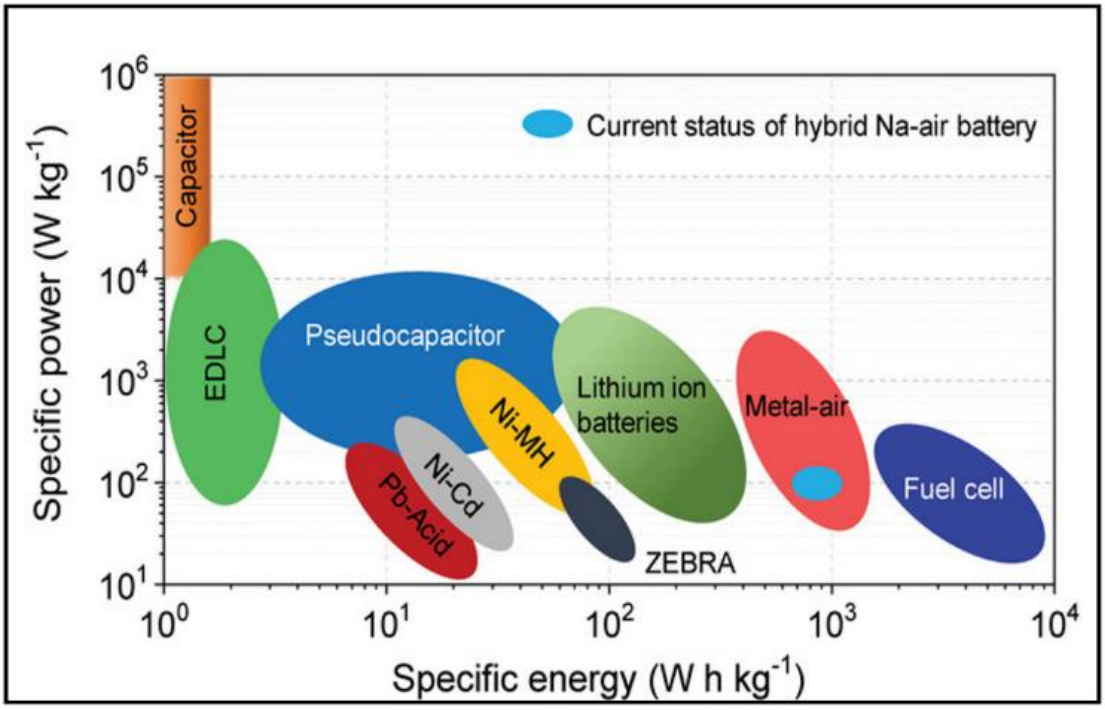

Figure 1.6 different types of energy storage technologies for stationary applications [27] (Figure is taken from open access internet source)

1.5.1 Battery is an alternating grid-scale energy storage solution

Battery stores electrical energy as chemical energy in two electrodes, a reductant (anode) and an oxidant (cathode), separated by an electrolyte that transfers the ionic component of the chemical reaction inside the cell and forces the electronic component outside the battery. The output on discharge is an external electronic current I at a voltage V for a time Δt. The chemical reaction of a rechargeable battery must be reversible on the application of charging I and V. Parameters of a rechargeable battery are safety, the energy density that can be stored at a specific power input and retrieved at a specific power output, cycle, and shelf life, storage efficiency, and cost of fabrication. Conventional ambient-temperature rechargeable batteries have solid electrodes and a liquid electrolyte. The positive electrode (cathode) consists of a host framework into which the mobile (working) cation is inserted reversibly over a finite solid−solution range. In a Li-ion battery, chemical energy is stored through redox-mediated intercalative reactions. The chemical energy is stored in the metal-ion battery through diffusion control redox. The working principle of the Li-ion battery is described in **figure 1.7.a.**[28] The most common rechargeable battery technology used in energy storage applications [29] is shown in **figure 1.7.b.**

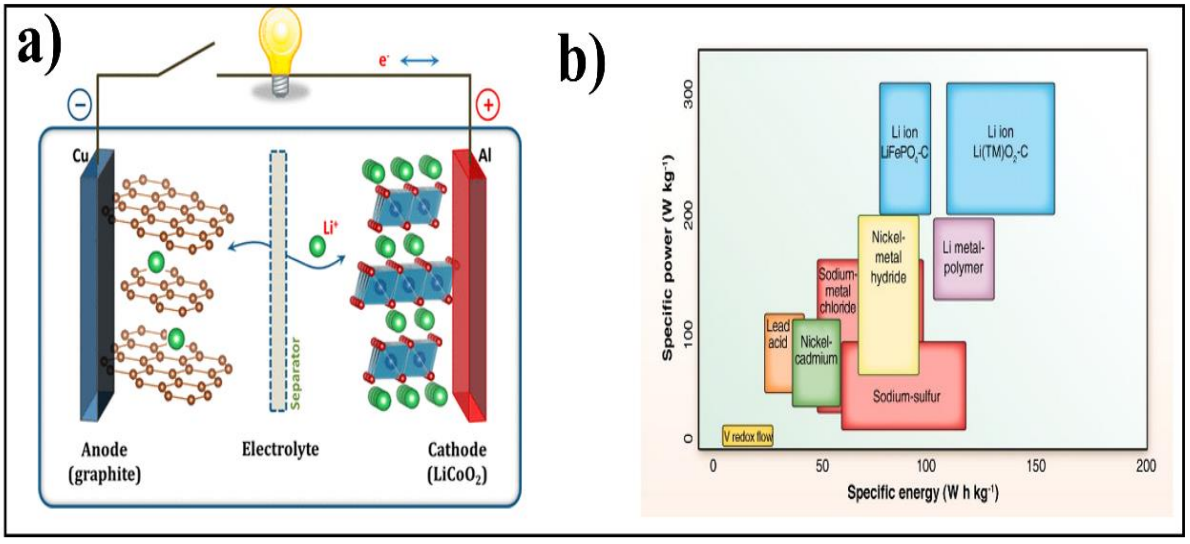

Figure 1.7 a) Schematic illustration of the first Li-ion battery ($LiCoO_2$/Li^+-ion electrolyte /graphite) [28] b) Gravimetric power and energy densities for different rechargeable batteries. Most of these systems are currently being investigated for grid storage applications [29] (Figure is taken from open access internet source)

1.5.2 Limitation of conventional metal-ion (Li-ion and Na -ion) battery

A wide range of issues lies in batteries that govern their performances and limitations in the desired application. The causes that can be addressed are given below, [30-32]

1. Based on transport and kinetic parameters

2. Capacity fade modelling (continuous or discontinuous)

3. Identification of unknown mechanisms

4. Low life to changing operating conditions

5. Heavyweight

6. Low power density

7. It is sensitive to high temperatures

8. Once the battery is completely discharged, it can no longer be recharged again.

1.6 Parameters of performances for grid-scale energy storage

The storage capacity and performance of an energy storage device can be defined [30-32]

1. UPS power quality

2. Grid supported

3. Bulk power.

A few suitable grid-scale energy storage technologies for different power and rate of discharge requirements are listed below and shown in **Figure1.8**. [30]

1. Redox flow battery

2. Metal-sulfur battery (Li-S, Na-S battery, etc.),

3. Metal-air battery (Li-air, K-air, Zn-air, etc.)

4. Pseudocapacitors (redox dominant metal oxide-based and interaction of metal ion /O^{2-}) application in supercapacitors application

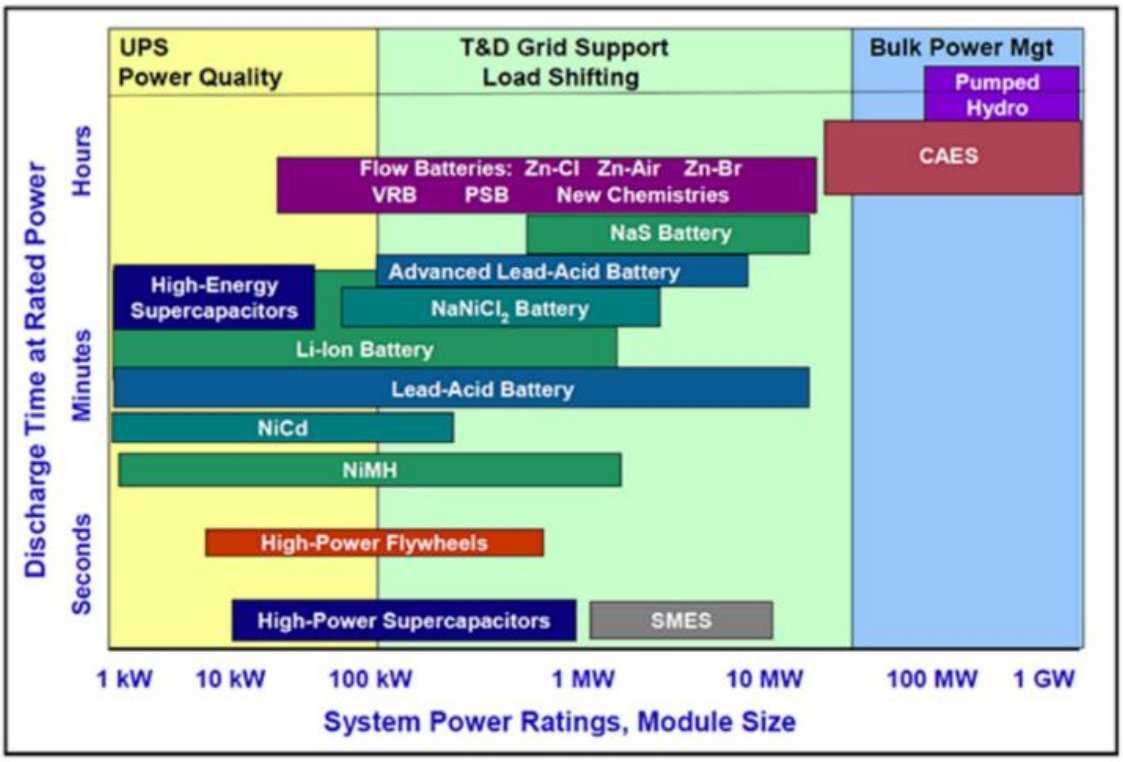

Figure 1.8 Suitability of energy storage technologies to different power and rate of discharge requirements (source: Sandia National Laboratories) [29] (Figure is taken from open access internet source)

1.6.1 Redox flow battery technology for grid-scale energy storage application

Redox flow batteries are promising energy storage candidates for grid-scale energy storage of intermittent renewable energy sources such as wind power and solar energy. Different new types of redox-active materials have been introduced and developed as cost-effective and high-power-density next-generation Redox flow batteries. Electrochemical kinetics play critical roles in influencing Redox flow battery performance like overpotential and cell power density. Redox flow battery technology is electrochemical energy storage that offers additional advantages over other storage systems, such as standalone modular design, no geographical requirement, high efficiency, fast response, etc. Of particular interest is the redox flow battery technology, its considered suitable for large-scale energy storage and has recently attracted considerable research interest because of several attractive features including long calendar life, simple design, and capability to withstand low

fluctuating power supply. Several redox-flow batteries have been developed using different active redox systems such as polysulfide/bromide, vanadium, Fe/Cr, etc. [33-36] **Figure1.9** shows a schematic of the mechanism of the vanadium redox flow battery

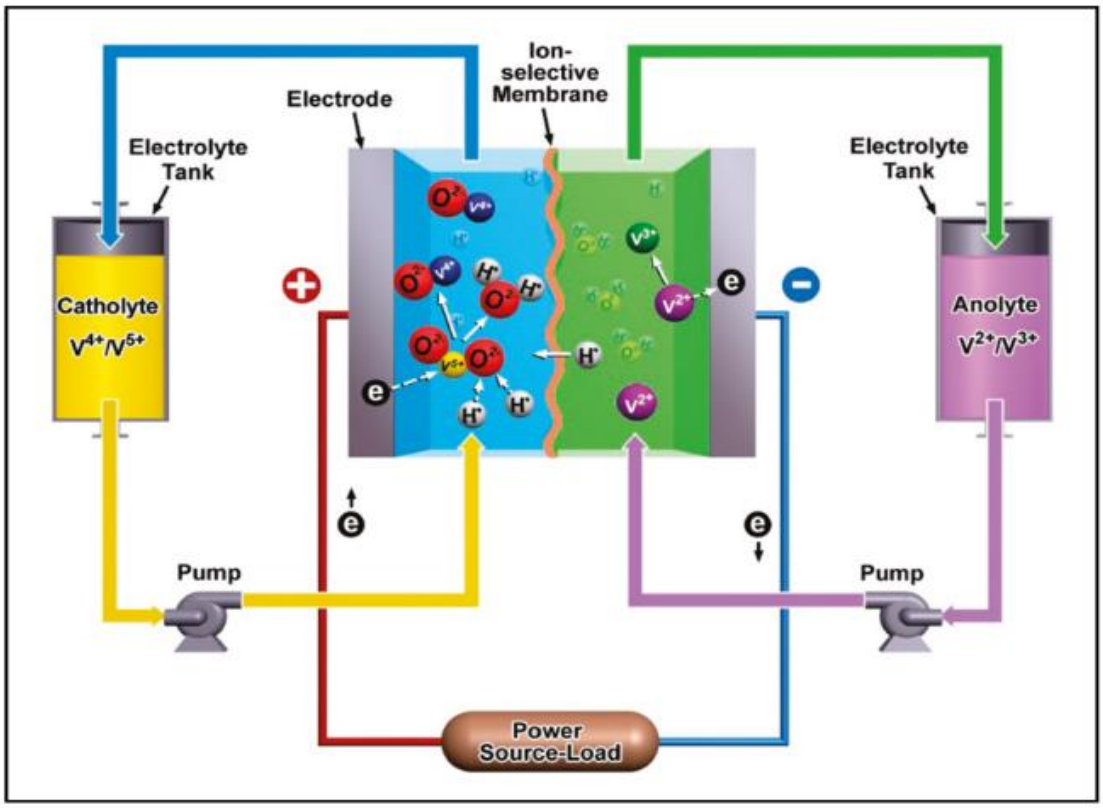

Figure1. 9 Schematic of the mechanism of vanadium redox flow battery [34] (Figure is taken from open access internet source)

1.6.2 Metal-sulphur battery technology for grid-scale energy storage application

In grid and transportation applications, electrochemical energy storage devices play a critical role because of their high energy density, long cycle, and calendar life, low cost, and high safety. Lithium-sulfur (Li–S) and sodium-sulfur (Na–S) batteries in a group of Alkali metal–sulfur batteries are a great potential for grid-scale application because of their extremely high energy density. Metal−sulfur batteries compose of the anode side is metallic and the cathode side is elemental sulfur impregnated in a porous matrix. They attract lot a of attention and are considered to be very next-generation batteries for the following reasons

1. Utilization of active metal anodes enables a leap in specific energy due to the high capacity of metal anodes in comparison to intercalation compounds,

2. Sulfur as a cathode exhibits high theoretical specific capacity (1.675Ah/g)

3. System components are low-cost and less toxic. The high reactivity of metallic anodes (e.g., Li, Na, Mg, and Al).

For example, the construction and Charge-discharge mechanism of the Li−S battery consists of a lithium metal anode, an organic electrolyte, and a sulfur composite cathode. Sulfur is in the charged state, the cell operation starts with discharge. During the discharge reaction, lithium metal is oxidized at the negative electrode to produce lithium ions and electrons. The lithium ions move to the positive electrode through the electrolyte internally while the electrons travel to the positive electrode through the external electrical circuit, and thereby an electrical current is generated. Sulfur is reduced to produce lithium sulfide by accepting the lithium ions and electrons at the positive electrode. [37-40]

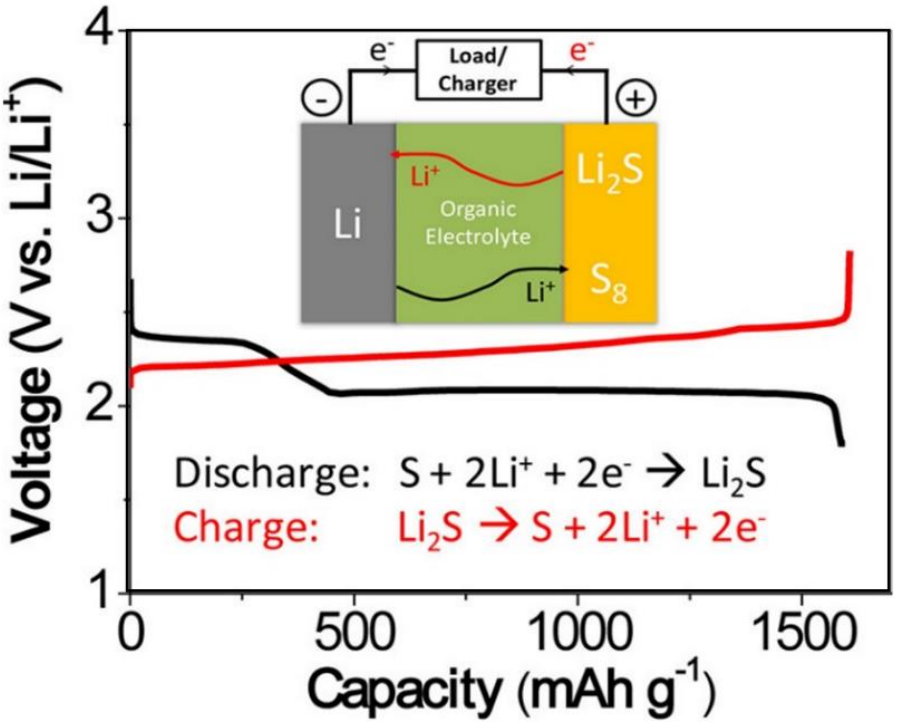

Figure 1. 10 Schematic diagrams of Li−S cell with its charge/discharge operations [40] (Figure is taken from open access internet source)

Figure 1.10 show Schematic presentations of a Li−S cell with its charge/discharge operations [41-42] The reactions occurring during discharge are given below, and the backward reactions will occur during charge.

Negative electrode: anodic reaction (oxidation, loss of electrons)

$$2Li \rightarrow 2Li^{+} + 2e \quad (1.1)$$

Positive electrode: cathodic reaction (reduction, gaining electrons)

$$S + 2Li^{+} + 2e^{-} \rightarrow Li_2S \quad (1.2)$$

Overall cell reaction

$$2Li + S \rightarrow Li_2S \quad (1.3)$$

The theoretical capacities of lithium and sulfur are 3.861 and 1.672 Ahg^{-1}, respectively, which leads to a theoretical cell capacity of 1.167 Ahg^{-1} for the Li−S cell. The discharge reaction has an average cell voltage of 2.15 V. Hence, the theoretical gravimetric energy density for a Li−S cell is 2.51 Whg^{-1}.[38]

1.6.3 Metal-air battery technology for grid-scale energy storage application

Metal-air batteries have much higher theoretical energy density than lithium-ion batteries and are frequently advocated as the solution for next-generation electrochemical energy storage for applications including electric vehicles or grid energy storage. Unfortunately, conventional lithium-ion technology based on intercalation chemistry is approaching its performance limit.

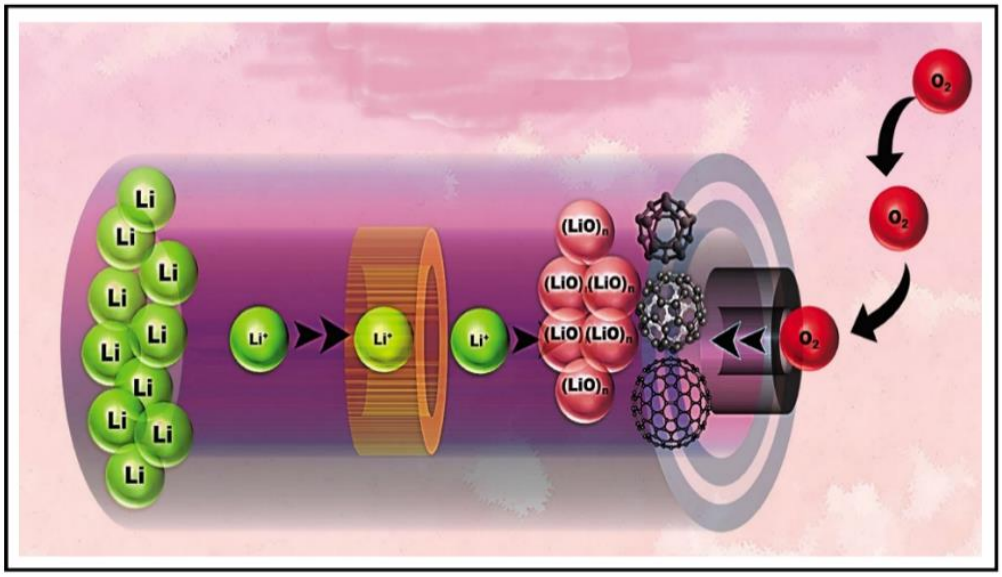

Figure 1. 11 Schematic diagrams of metal-air battery (e.g- Li−air battery) [46] (Figure is taken from open access internet source)

Among grid-scale candidates, metal-air batteries have gained revived interest because of their energy density. Metal-air batteries are assembled with a metal anode and an air-breathing cathode in a proper electrolyte. The metal anode can be alkali metals (e.g. Li, Na, and, K), alkaline earth metals (e.g. Mg) first-row transition metals (e.g. Fe and Zn) with good electrochemical equivalence; the electrolyte can be aqueous or non-aqueous – depending on the nature of the anode employed; the air-breathing cathode often has an open porous architecture that permits continuous oxygen supply from surrounding air.[43-47] **Figure 1.11** shows schematic diagrams of the Li−air battery.

1.6.3.1 Development of metal-air battery

Zn-air battery was the first invention of the metal-air battery in 1878 by L. Maiche [48], then continuously progress was happed in metal-air battery different like Al-air battery (1962), Fe-air battery (1978), Li-O_2 battery (1996) and latest proposed was in 2018 water in salt in Zn-O_2 and Li-O_2 battery.[48-64]

1.6.3.2 Type Metal-air batteries

Different types of metal-air batteries (Li, Na, Mg Zn, Al, and Fe (anode material) – air (cathode)) were proposed in different time scales. Theoretical energy density is an important factor in evaluating the performance of various battery configurations. **Figure 1.12** shows the theoretical energy density, specific energy, and nominal cell voltage of different types of metal-air batteries. As oxygen, directly supplied from the surrounding environment, is involved in the cathode as an oxidant during the discharge period, metal-air batteries show considerably higher energy density. Although, theoretically, lithium-air batteries offer the best combination of the highest theoretical energy density (5928 Wh kg^{-1}) and high cell potential (nominally 2.96 V), iron–air batteries have the smallest theoretical energy density and cell voltage (nominally 1.28 V). Al-, Zn-, and Fe–air batteries are also the research hotspots because of their economics and safety parameters.[65]

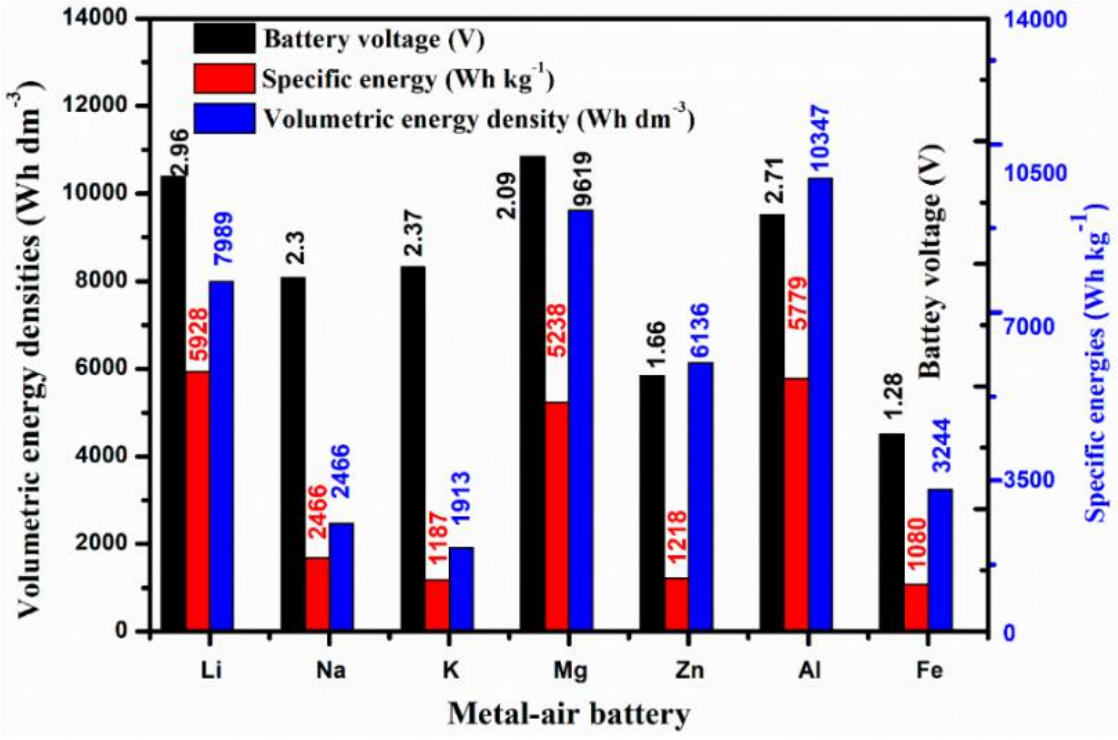

Figure 1. 12 Theoretical energy density, specific energy, and nominal cell voltage of different types of metal-air batteries [65] (Figure is taken from open access internet source)

1.6.3.3 Metal anode and Working principle of the metal-air battery

The working principle of Metal –air battery differs from that of traditional metal-ion intercalative batteries. The traditional intercalative batteries involve the transformation of metal ions from the anode to the cathode. In Metal –air battery, metals or alloys transform into metal ions at the anode and oxygen transforms into oxide or hydroxide ions at the cathode.

Figure 1.13 shows the schematic of a Metal–air battery in an aqueous or non-aqueous electrolyte medium. In an aqueous electrolyte system, oxygen diffuses into batteries through the gas diffusion layer and transforms into hydroxide-ion receiving electrons. In a non-aqueous electrolyte system, oxygen receives electrons and transforms into an oxide-ion. Metals release electrons, transform them into metal ions, and dissolve into electrolytes. These processes will be reversible during a charging procedure of a rechargeable Metal –air battery [66-69]

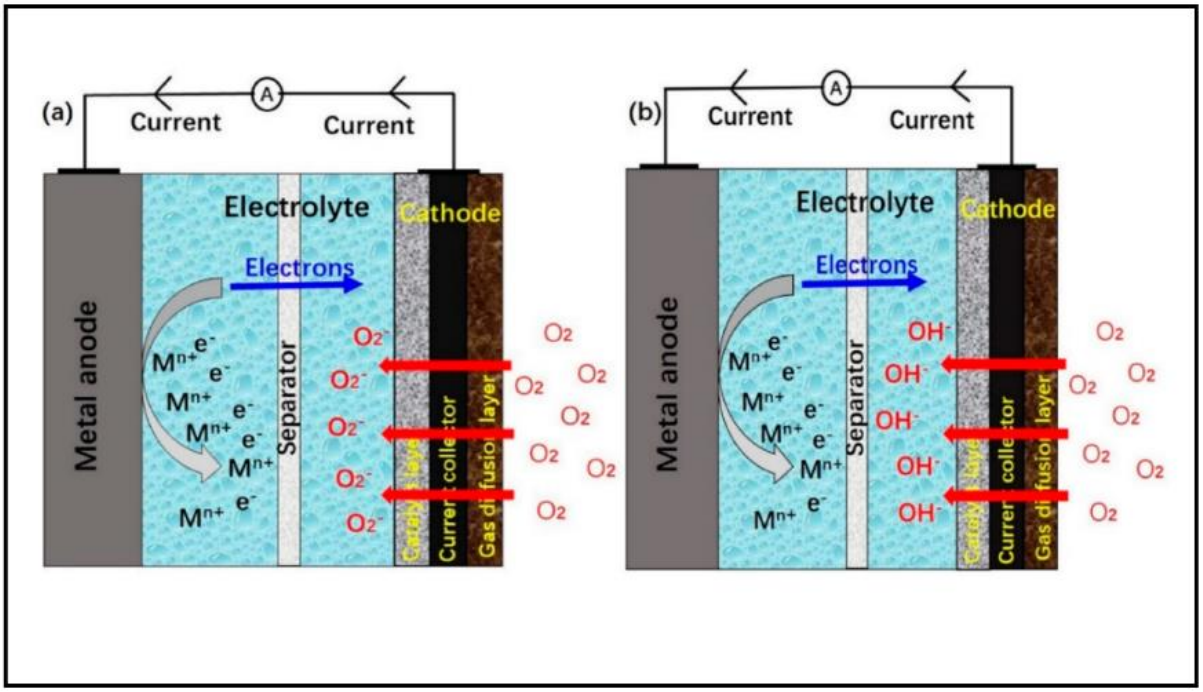

Figure 1. 13 Schematic diagrams of Metal-Air Batteries working principles for (a) non-aqueous electrolyte, and (b) aqueous electrolyte.[65] (Figure is taken from open access internet source)

The electrochemical reaction of metal (Fe, Al, Zn) and oxygen in metal-air batteries are described below.

In **Aqueous electrolyte**

$$\textbf{Anode}: M \rightleftharpoons M^{n+} + ne- \quad (1.4)$$

$$\textbf{Cathode}: O_2 + 2H_2O + 4e- \rightleftharpoons 4OH \quad (1.5)$$

Non-Aqueous electrolyte

The working principle of Li-air battery in the non-aqueous electrolyte is given below. [69]

$$\textbf{Anode}: Li \rightleftharpoons Li+ + e- \quad (1.6)$$

$$\textbf{Cathode}: O_2 + e- \rightleftharpoons O^{2-} \quad (1.7)$$

$$O^{2-} + Li+ \rightleftharpoons LiO_2 \quad (1.8)$$

$$LiO_2 + Li+ + e- \rightleftharpoons Li_2O_2 \quad (1.9)$$

$$\textbf{Overall reaction}: O_2 + Li \rightleftharpoons Li_2O_2 \quad (1.10)$$

1.6.3.4 Air cathode and role of cathode supported OER (Oxygen Evolution Reaction) and (Oxygen Reduction Reaction) ORR catalyst

Metal–air battery consists of a high energy density anode (Li, K, and Zn) and a fuel cell-like air cathode. Air cathode-supported ORR catalysts are very important in developing energy storage systems, and the catalyst also expedites the chemical reactions and improves the yield of the product due to its capability of suitably changing the process and progress of the reaction by lowering the activation energy. Catalyst`s ability for efficient air cathodes, that is, for ORR and OER processes, requires high electronic conductivity, non-solubility in an aqueous acidic or basic medium, optimal porosity for fast oxygen diffusion, and selective adjustments of hydrophobic and hydrophilic properties for the ORR and OER processes.[70-79] During battery discharge in an alkaline electrolyte, the metal anode reacts with OH^- to oxidize it. At the same time, oxygen in the air diffuses into the porous air cathode and then is reduced to hydroxide ions at the three-phase interface. [80]

Oxygen Reduction Reaction (ORR), $O_2 + 2H_2O + 4e^- \rightarrow 4OH^-$ (1.11)

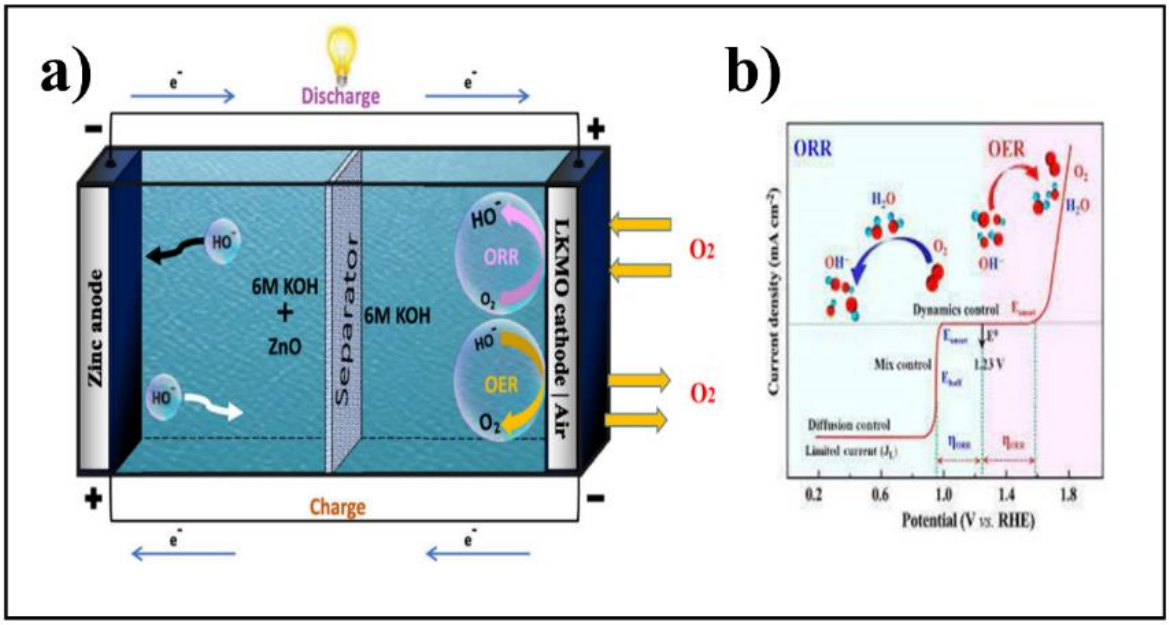

Figure 1. 14 Schematic diagrams of a) working principle of Zn−air battery[82] and b) OER and ORR mechanism on air cathode [83] (Figure is taken from open access internet source)

Subsequently, the generated OH^- species will migrate from the air cathode to the metal anode in the electrolyte, thereby completing the entire charging reaction. As for the charging process, the metal salt is reduced to metal at the metal electrode and the oxygen release reaction occurs at the air electrode [81]

Oxygen Evolution Reaction (OER), $OH^- \rightarrow O_2 + 2H_2O + 4e^-$ (1.12)

At present, the ORR reaction and OER reaction rate at the air electrode are the key factors limiting the rechargeable metal-air battery. Understanding the reaction mechanism and process is essential to designing an effective bifunctional catalyst. **Figure 1.14** shows schematic diagrams of the Li−air battery and OER and ORR mechanism. [82-83]

1.6.3.4 .1 Overpotential

Overpotential is the most effective tool for evaluating the effectiveness of the ORR and OER catalysts. The value of the overpotential at 10 mA/ cm^2 (Ej=10) is commonly used for the study of developing efficient OER/ORR catalysts.[84] Overpotential represents the energy barrier of the reaction. In general, the onset

potential and half-wave potential (E/2) are evaluated for ORR and the onset potential and the potential at 10 mA/cm^2 (Ej_{10}) are evaluated for OER. To have a more direct evaluation of activity in the bifunctional catalyst,

$$\Delta E = Ej_{10} - E1/2 \quad (1.13)$$

It is more indicative of the common overpotential of ORR and OER and is also closely related to the open circuit potential of the metal-air battery. [85]

1.6.3.4 .2 Tafel slope

Tafel proposed empirical formula in 1905 known as the Tafel formula and he established mathematical expressions between Overpotential and Exchange Current density. [86]

$$\boldsymbol{Over\ potential}\ , \eta = Alog_{10}\frac{j}{j_0} \quad (1.14)$$

η = overpotential,

A = Tafel slope

j = current density, mA/cm2

j_0 =Exchange current density", mA/cm2.

The kinetic process and mechanism of electrocatalysis can be analyzed from the Tafel slope. The lower it is, the smaller the driving force required for the reaction process, which applies to both ORR and OER. An excellent bifunctional catalyst should have a low Tafel gradient when undergoing ORR and OER.[84-86]

1.6.3.4 .3 Exchange current density (i_0)

The exchange current density j_0 is a thermodynamic concept that reveals the nature of the electrode reaction. In addition to being affected by temperature, it is also related to electrode materials and the concentration of reactive substances and electrolytes. The value can be calculated according to the Tafel curve. The internal factor in the polarization degree of the electrode (overpotential) depends on the exchange current density. If the exchange current density is large, the driving force (external current density) required for one electrode reaction is small. If the exchange current density

is small, the driving force (external current density) required for one electrode reaction is large.[87-88]

1.6.3.5 Survey of OER (Oxygen Evolution Reaction) and (Oxygen Reduction Reaction) ORR catalysts with different lattice structures

Figure 1.15 present the improvement of the real OER catalyst (blue) in direct relation to the shift in the chemisorption free energy of the peroxo species OOH (adsorbed). ΔGOOH(adsorbed) shifted to more negative values, resulting in a stronger surface bonding until equally spaced reaction-free energies are obtained (red).[89] The involvement of multiple intermediates makes the full kinetic analysis of OER on metal oxides a daunting task. A volcano-type relation of the activity of OER catalysts as a function of ΔGOOH(adsorbed) is identified recently. [90]

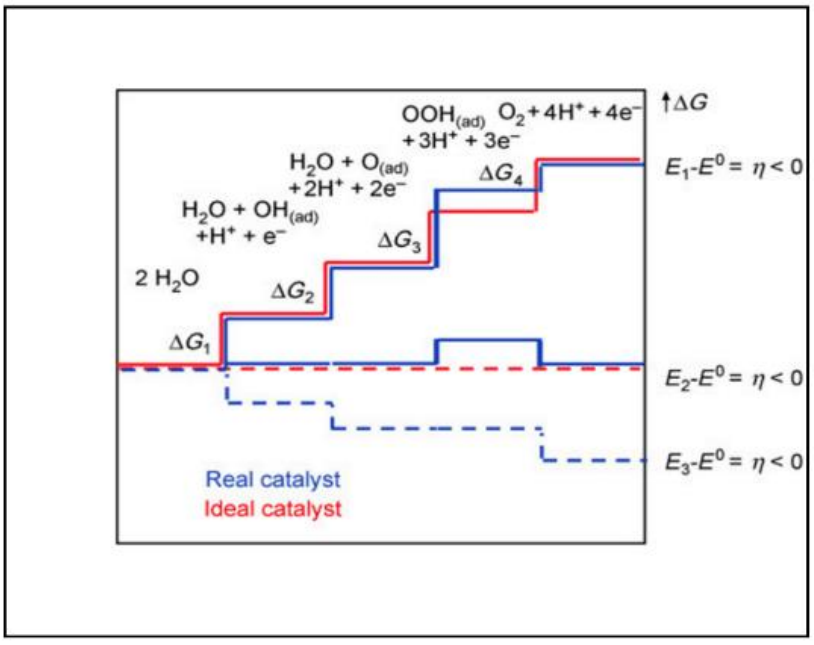

Figure 1. 15 Schematic diagrams of Gibbs free energy of reactive species and intermediates (horizontal lines) of the oxygen evolution reaction (OER) versus the reaction coordinate. Blue lines and red lines indicate the energetics of a real (typical) catalyst and an ideal catalyst, respectively. [89] (Figure is taken from open access internet source)

1.6.3.5.1 OER and ORR activity of transition/noble metal oxides

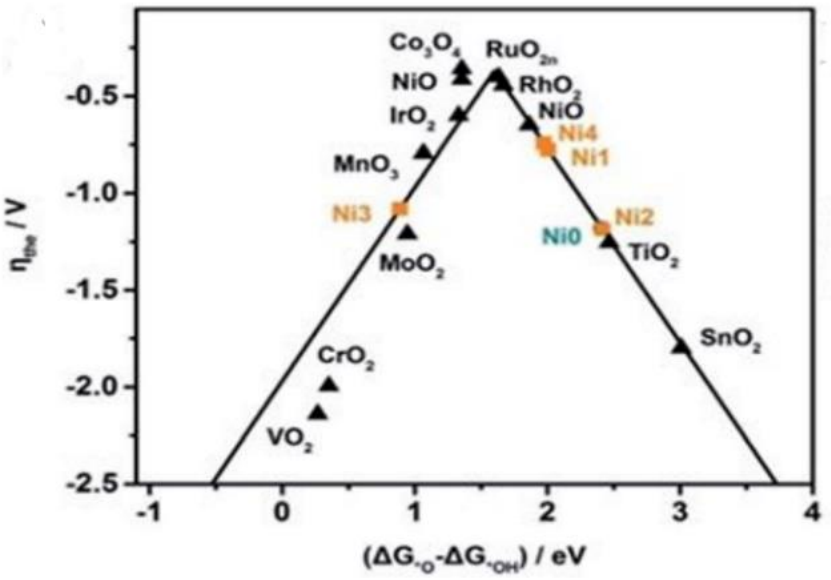

Figure 1. 16 Schematic diagrams of Volcano plots of common metal electrocatalysts [95] (Figure is taken from open access internet source)

Figure 1.16 show the schematic diagrams of the Volcano plot of common metal electrocatalysts concerning −OH bonding strength stabilizing IrO_2 and RuO_2 at the top of the volcano. [91-93] The OH^--$M^{2+\delta}$ bond strength followed the order of Ni < Co < Fe < Mn, which correlated well with the OER activity order (Ni > Co > Fe > Mn).[94,95] Bifunctional activity of MnOx-based type catalysts depends on oxidation states, crystal structures, and surface area. For e.g. MnO_2 has different polymorphic forms such as α form- cryptomelane, β form- rutile, γ form- manganite, and δ form- vernadite types. It has been shown in several studies that catalytic activity of the polymorphic MnO_2 is in the sequence β-MnO_2 < λ-MnO_2< γ-MnO_2 < α-MnO_2 ~ δ MnO_2. [96-101]

1.6.3.5.2 Role of e_g electron on ORR/OER activity of Spinel and perovskite-type oxide materials

Chao Wei et al. observed that the e_g electron occupancy of the active cation in the octahedral site is the activity descriptor for the ORR/OER of the spinel structure. Activity on spinel as a function of the M (Metal) valence state of the active element at the octahedral site resulted in a volcano shape, as displayed in **figure1.17 (a-b).**

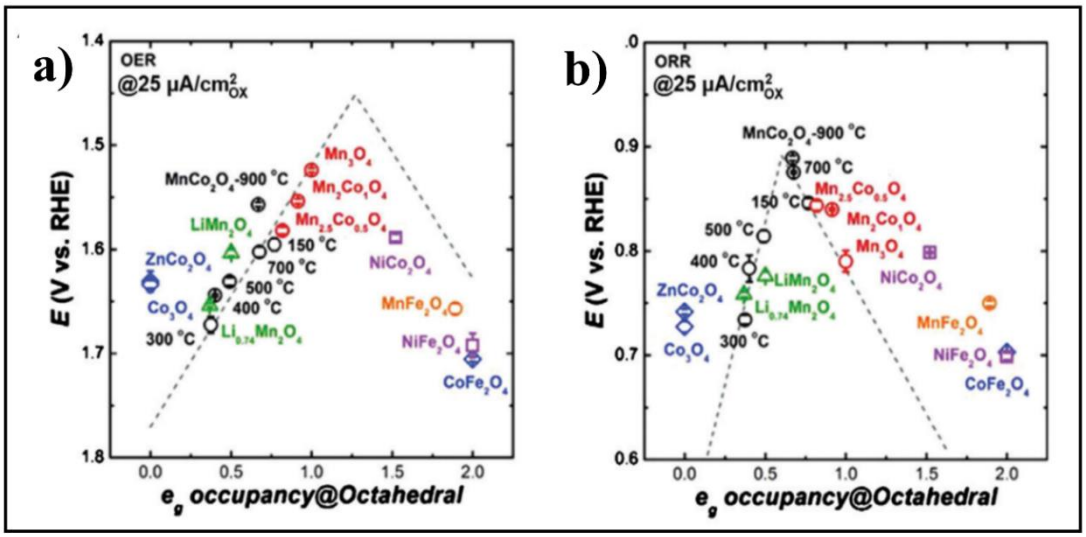

Figure 1. 17 (a-b) Schematic diagrams of Volcano plots ORR and OER activity respectively on various spinels as a function of eg occupancy of the active element at the octahedral site. [102] (Figure is taken from open access internet source)

The role of an e_g electron at the octahedral site can be explained by the four-step proton/electron-coupled reaction mechanism.[102-105] Volcano shape demonstrates the applicability of the ORR/OER activity prediction of transition-metal spinel structure e_g filling of the octahedral element and the occupation of the active element at the octahedral site simultaneously govern oxygen electrocatalysis. The ORR/OER activity can be optimized at a moderate eg filling ($e_g \approx 1$) at the octahedral site, which balances the competition between rate-limiting steps. [102-115]

Electronic structure parameters have been used as descriptors for perovskite (ABO_3 where A= alkaline rare earth B= transition metal) catalysts for OER /ORR activity. Bockris established the OER /ORR activity of perovskites with the number of 3d electrons of the transition metal ions in bulk perovskites. [116-118] Relevant metal orbitals of first-row transition metals show in BO_5 octahedral (oxygen-deficient perovskite) configuration and electrons from the d-orbitals showed different transition metals occupying the antibonding (e_g) orbitals as shown in **figure 1.18**.[118] M−OH bond strength depends on the number of d electrons, increase in d electrons, decreases the bond strength of M−OH, and the increases OER activity. Shao-Horn first proposed that the surface filling of e_g orbitals improved catalytic activity of perovskites materials as shown in **figure 1.19.**[104] Compared to 3d electrons counts, e_g filling is in principle more appropriate because the e_g orbitals have more direct

overlap with the oxygen-related adsorbate than t_{2g} orbitals. Moreover, as electrocatalysis occurs at the surface, a surface-based parameter is more accurate than a bulk parameter. The volcano plot was obtained using the e_g filling as a descriptor, with the optimal values being close to unity. $Ba_{0.5}Sr_{0.5}Co_{0.8}Fe_{0.2}O_{3-\delta}$ (BSCF) had a near-optimal e_g filling, and BSCF was indeed the best perovskite catalyst. For perovskites whose e_g filling is hard to estimate, e.g., double perovskites with multiple transition metal sites, Shao-Horn proposed the computed Oxygen p-band center relative to the Fermi level as an alternative descriptor .[119]

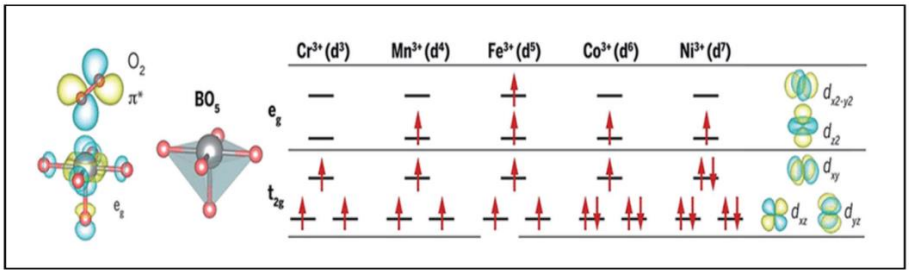

Figure 1. 18 Electronic configurations (d orbital spitting bonding (t_{2g})) and antibonding (e_g)) and relevant metal orbitals of first-row transition metals for a BO_5 configuration.[116] (Figure is taken from open access internet source)

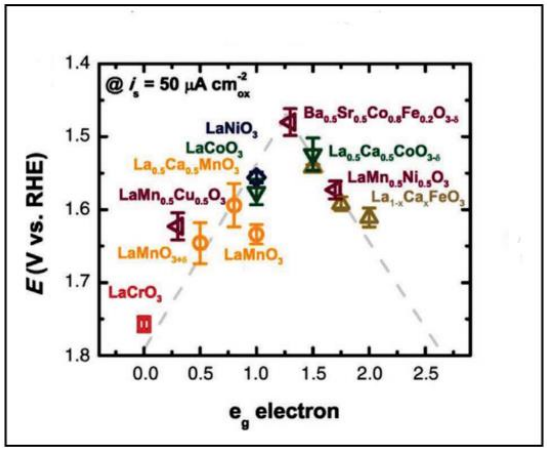

Figure 1. 19 The relation between the OER catalytic activity, defined by the overpotentials at 50 μA cm−2 of OER current, and the occupancy of the eg-symmetry electron of the transition metal (B in ABO_3).[119] (Figure is taken from open access internet source)

1.6.3.5.3 Role of e_g electron on ORR activity of Perovskites (ABO_3) metal oxides

ORR activity of Perovskites metal oxide (ABO_3) depends on the number of 3d-electrons of B-site ions and ORR activity with the hypothesis that the number of 3d-electron represents the antibonding electron occupation of the B–O bond.[120]. The comparison between the ORR activity of the perovskites and the d-electron number per B cations shown in **figure 1.20 a)** reveals an M-shaped relationship with the maximum activity attained near d^4 and d^7. The intrinsic ORR activity of all the oxides exhibits a volcano shape as a function of the e_g-filling of B-site cations. This is supported by the correlation between increasing e_g filling and decreasing onset temperature for oxygen release (measured by O_2 temperature-programmed desorption), in the order $LaCrO_3$ (e_g =0).$LaMnO_3$ (e_g=1) ≈ $LaCoO_3$ (e_g ≈ 1) ≈ $LaNiO_3$ (e_g ≈ 1) and $LaFeO_3$ (e_g =2), which is indicative of the strength of bonding between B-site cations and oxygen. Partial substitution on the A or B sites features charge compensation via oxygen vacancy or changing of the B-ion valency in the e_g electron occupancy calculation of surface B ions. ORR activity as a function of e_g-filling produces a definitive volcano plot as shown in

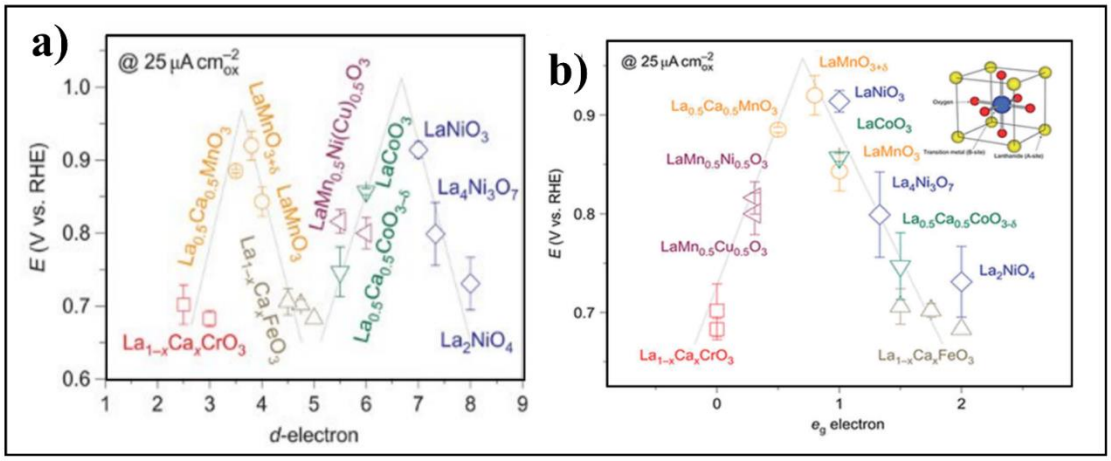

Figure 1. 20 a) Potentials at 25 mA/ cm2 of the perovskite oxides have an M-shaped relationship with the d electron number [120] b) Role of eg electron on ORR activity of perovskite oxides, Potentials at 25 mA cm22 as a function of eg orbital in perovskite-based oxides. [120] (Figure is taken from open access internet source)

Figure1. 20 b) with a voltage span of 0.25 V. The ORR activity in e_g-filling $La_{1-x}Ca_xCrO_3$ ($t_{2g}^3e_g^0$ for x = 0, $t_{2g}^{2.5}e_g^0$ for x = 0.5) can result in B–O_2 bonding that is too

strong, whereas much eg-filling in $La_{1-x}Ca_xFeO_3$ ($t_{2g}^3e_g^2$ for x=0, $t_{2g}^3e_g^{1.75}$for x =0.25, $t_{2g}^3e_g^{1.5}$for x = 0.5) B-O_2 interaction is too weak resulting the situation optimum for ORR activity. On the other hand, a moderate amount of eg-filling (≈1) in $La_{1-x}Ca_xMnO_3$ ($t_{2g}^3e_g^1$for x=0, $t_{2g}^3e_g^{0.5}$ for x = 0.5), $LaCoO_3$ ($t_{2g}^5e_g^1$) and $LaNiO_3$ ($t_{2g}^6e_g^1$) shows the highest activity.[118-119]

1.7 Pseudocapacitors or Supercapacitors for grid-scale energy storage application

The current success of Pseudocapacitors is in large part due to the use of transition metal oxides in one or both electrodes. Transition metal oxide materials exhibit pseudocapacitance, which arises when reversible redox reactions occur at or near the surface of a material in contact with an electrolyte. [120] Advantage of supercapacitors using pseudocapacitive electrode over metal (Li, Na)-ion battery is shown in **figure1.21.** Supercapacitors provide higher power and longer cycle life than that batteries and are receiving renewed attention for grid-scale energy storage applications [121-127]

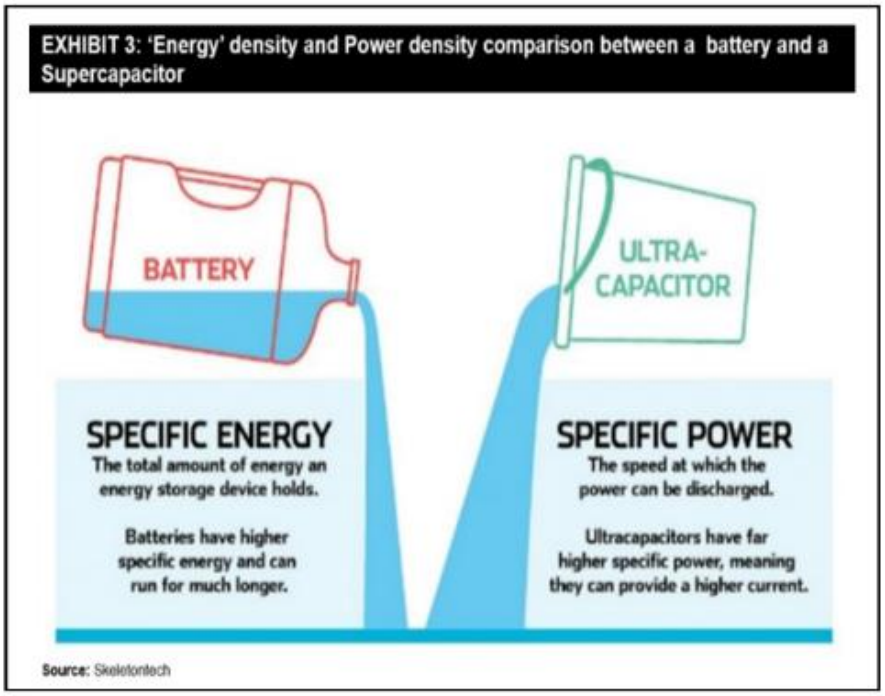

Figure 1.21 Advantage of supercapacitors over battery [123] (Figure is taken from open access internet source)

1.7.1 Development of pseudocapacitors

Discovering charge-storage mechanisms on metal oxide was started in the 18th century. The first capacitor, named a "Leyden jar", was invented separately by a German cleric Ewald Georg von Kleist in 1745 and a Dutch scientist Pieter van Musschenbroek in 1746. In the early 1960s, Conway and Gileadi observed that pseudocapacitance behavior arises from electrochemical charge transfer reactions associated with surface adsorption. Pseudocapacitance is followed by the Langmuir adsorption model. Capacitance arises from Faradaic reactions that involved monolayers of electrochemically active species. these phenomena distinguish pseudocapacitance from double-layer capacitance.[128-135] Historical development in the field of pseudocapacitance is shown in **Figure 1.22.** Ruthenium oxide (RuO_2) thin film in sulphuric acid was first successfully reported as pseudocapacitive electrode materials by Trasatti and co-workers in 1971.[128] Pseudocapacitance due to proton transport was observed first in hydrated RuO_2 ($RuO_2 \cdot 0.5H_2O$). Nanostructure of RuO_2 with

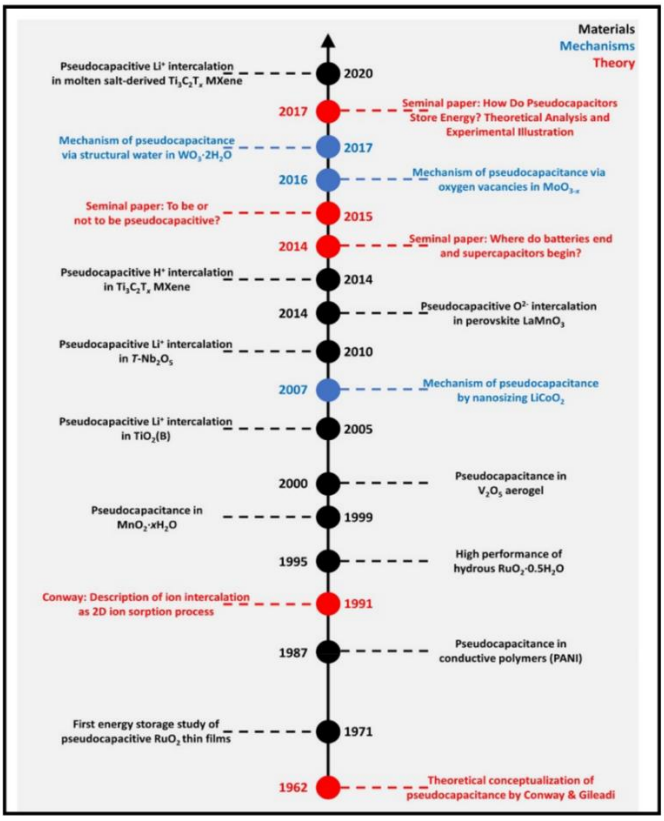

Figure 1.22. Timeline of major developments in the field of pseudocapacitance [142] (Figure is taken from open access internet source)

increased interfacial area showed superior activity due to superior interaction between the electrode and the electrolyte and reactive sites that were accessible for charge transfer reactions.[130-131] Conducting polymers showed pseudocapacitive charge storage properties and lots of materials were established by Shirakawa et al.the in late 1980s.[132] Conway in the early 1990s shows the pseudocapacitive nature of Li^+ intercalation in a 2*d* ion sorption process in between layers of transition metal oxides and sulfides.[133-139] Goodenough group in 1999 also reported that an amorphous, hydrated $MnO_2 \cdot xH_2O$ showed capacitor-like behavior in neutral pH aqueous KCl electrolytes in a potential window of 1.2V.[140] Levi and Aurbach also proposed modeled Li^+ intercalation in terms of a Frumkin intercalation isotherm.[141] Zukalová et al. reported that Li^+ storage in the monoclinic bronze structure titanium oxide TiO_2 (B) and show that the charge storage mechanism is pseudocapacitive in nature.[142] Augustyn et al. reported that Li^+ intercalation in T-Nb_2O_5 exhibits pseudocapacitors-like kinetics.[144] This was attributed to rapid transport along two-dimensional planes and no intercalation-induced phase changes over a wide range of Li^+ storage in the host lattice.[145]

1.7.2 Classification of Pseudocapacitance

The kinetic theory of pseudocapacitive storage assumed a linear dependence of the heat of adsorption on the surface coverage of the electrodeposited species and led to a capacitance defined in terms of the surface coverage. Conway observed pseudocapacitance behavior and adsorption of monolayer H^+ ion on the surface is followed by Langmuir Adsorption as shown in **Figure1.23 (a, d)**.[146-147] Faradaic reactions mechanism occurs in hydrous RuO_2 in H_2SO_4 (redox pseudocapacitance) as shown in **Figure1.23 (b,e).**[148-149] Pseudocapacitive type Li-ion intercalation was shown in Nb_2O_5 in Figure **1.23 (c, f).**[150] The extent of reaction (based on the surface coverage, surface redox, or intercalation) depends almost linearly on the potential (V).

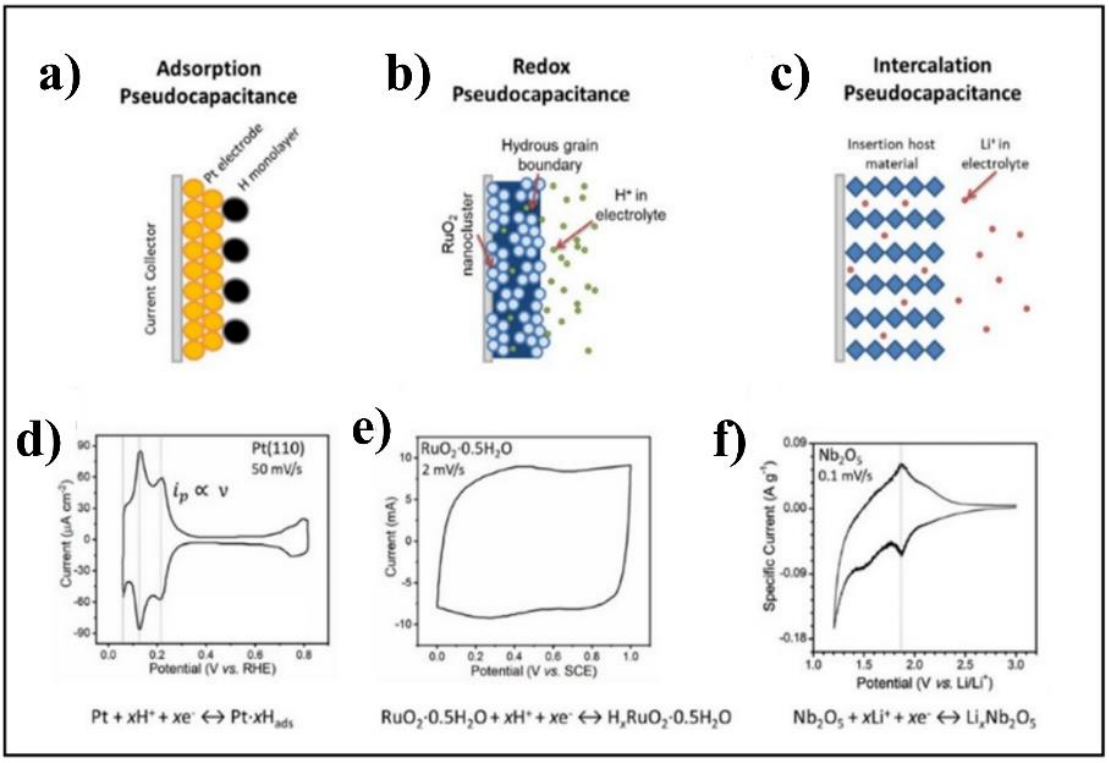

Figure1.23.a) Adsorption pseudocapacitance, b) redox pseudocapacitance, and c) intercalation pseudocapacitance. d) CV of a Pt. (110) surface in aqueous 0.1M$HClO_4$ solution at 50mV/s E) CV of a $RuO_2 \cdot 0.5H_2O$ electrode in aqueous 0.5MH_2SO_4 solution f) CV of T-Nb_2O_5 Nano crystalline film in a nonaqueous Li^+ electrolyte cycled at 0.1 mV/s. [139,146-150] (Figure is taken from open access internet source)

1.7.3 Psedocapative materials with different lattice structures

For the fundamental understanding of pseudocapacitance, hydrous RuO_2 ($RuO_2 \cdot nH_2O$), iridium oxide (IrO_x), and MnO_2 (typically birnessite δ-MnO_2, of the type $K_xMnO_2 \cdot nH_2O$) are among the best-studied materials exhibiting pseudocapacitive charge storage. [156-157]. Over the last few years, metal oxides such as single metal oxides (such as Fe_2O_3, V_2O_5, RuO_2, MnO_2, MoO_3, and WO_3), bimetallic oxides (conversion-type AB_2O_4, A, or B denote = Ni, Co, Zn, Mn, Fe, Cu, etc. and intercalation-type ($LiCoO_2$, $LiMn_2O_4$, etc.)) and metal oxide heterostructures, have been widely investigated as electrode materials for pseudocapacitors applications [151-157]

1.7.3.1 Fe-O_x redox mediator type materials

Iron oxides, particularly Fe_2O_3 and Fe_3O_4, have attracted widespread attention as potential anode materials for pseudocapacitor applications. Yan et al. designed an

electrode material using Fe_3O_4 nanospheres decorated on graphene Nano-sheets via a facile solvothermal procedure and showed high pseudocapacitive energy storage capacity.[159] When assembled as an anode for supercapacitors, the fabricated graphene/Fe_3O_4//graphene/MnO_2 AASCD displayed an excellent energy density of 87.6 $Whkg^{-1}$.[158]

1.7.3.2 VOx-based redox mediator type materials

Vanadium-based oxides have the merits of achieving high power density and natural abundance with high theoretical specific capacity. Nevertheless, unsatisfactory structural stability and poor electric conductivity block their application. Vanadium oxides mainly include VO_2, V_2O_3, and V_2O_5, where the +5 state is the most stable and +4 is the worst. As an electrode material, V_2O_5 has been widely investigated as a pseudocapacitivecathode material.[159]

1.7.3.3 MnOx-based redox type materials

Manganese oxide materials have been broadly investigated for cathode materials. MnO_2 and Mn_3O_4 have attracted considerable attention for applications owing to their low cost, wide operating potential window, and earth abundance nature. Zhang et al. reported a core-shell pseudocapacitors electrode of a b-MnO_2 core and highly aligned "birnessite-type" MnO_2 shell. A high energy density of 40.4 $Whkg^{-1}$ with a maximum power density of 17.6 $kWkg^{-1}$.[160-161]

1.7.3.4 RuO_2-based Redox mediator type materials

RuO_2 is considered a model host structure for pseudocapacitive charge storage due to its high theoretical specific capacitance (1700 Fg^{-1}), good electrical conductivity (105 $S.cm^{-1}$), and reversible redox reaction. RuO_2 is recognized as one of the most promising pseudocapacitive electrodes. RuO_2 has good corrosion resistance to acidic and basic environments, promising wide applications for aqueous systems in different aqueous electrolytes.[154-155]

1.7.3.5 CoO_x-based Redox mediator type materials

Among a variety of cobalt oxides, Co_3O_4 cathode materials are controlled by diffusion in the electrochemical process in an aqueous electrolyte and are considered battery-type electrode materials. The Co_3O_4 cathode has been vigorously developed due to its ultrahigh-specific theoretical specific capacitance and impressive redox reversibility.

Therefore, considerable endeavors have been concentrated on designing nanostructured Co_3O_4 materials to improve electrochemical performances. Yu et al. reported Co_3O_4/N-doped carbon hollow spheres with a hierarchical nanostructure as an advanced electrode for a high-performance asymmetric supercapacitors device. [162] Other metal oxide materials have been studied for pseudocapacitors electrodes, including MoO_3, [163] WO_3, [164] PbO_2, [165] SnO_2 [166], and CuO [167] NiO is a potential anode material for supercapacitors. Wei et al. synthesized honeycomb-like mesoporous NiO microspheres via a hydrothermal reaction as a high-performance cathode material [168].

1.7.3.6 TiO_2 (B) cationic intercalation type materials

Monoclinic bronze titanium dioxide (TiO_2 (B)), first described by Marchand et al. in 1980, is a metastable polymorph of titanium dioxide, which can be synthesized by hydrolysis and subsequent dehydration of alkali titanates. The TiO_2 (B) phase has the highest theoretical Li^+ intercalation capacity of all titania polymorphs Li_xTiO (B), with $x < 1.25$, which has a theoretical capacity of 419 mAh/g.[169-170]

1.7.3.7 T-Nb_2O_5 cationic intercalation type materials

Nb_2O_5 has been investigated as a Li^+ intercalation host since the 1980s. It can exist as several polymorphs, forming a pseudo-hexagonal structure around 500°C (TT-Nb_2O_5), an orthorhombic structure around 800 °C (T-Nb_2O_5), a tetragonal (B−Nb_2O_5) structure around 1000 °Cn and a monoclinic structure above 1100 °C (H-Nb_2O_5).[158] Kumagai et al. discovered that lithiation of T-Nb_2O_5 occurs via a solid-solution formation process below 2V vs. Li/Li^+, forming $Li_xNb_2O_5$ up to $x \leq 2$ resulting in a superior pseudocapacitive performance shown in **figure 1.24**. [171-174]

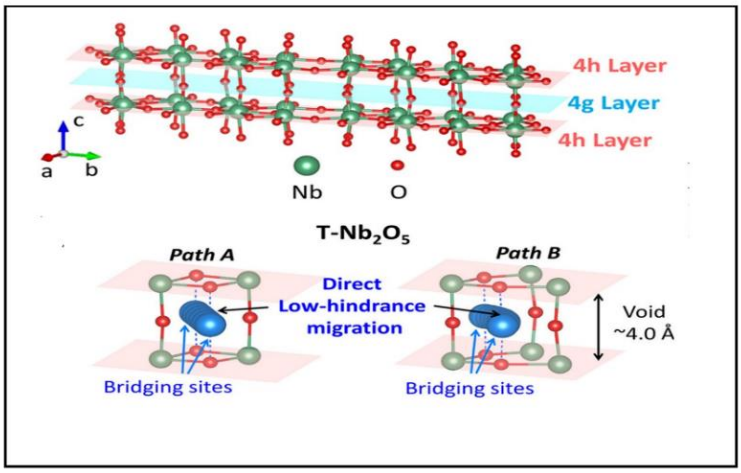

Figure 1.24. Structural model of T-Nb_2O_5, highlighting densely packed 4h layers and loosely packed 4g layers and proposed low-hindrance Li+ diffusion paths between bridging sites.[172] (Figure is taken from open access internet source)

1.7.3.8 Perovskite Oxides anionic intercalation type materials

The perovskite with formula ABO_3, where A is usually a lanthanide or an alkali earth metal and B is a transition metal (Fe, Co. Mn, Ni, etc.) are well-known materials in energy conversion applications such as electrocatalysts in solid oxide fuel cells.[175] Kudo et al first explore that the perovskite materials have excellent electrochemical energy storage properties also. The reported material was oxygen-deficient $Nd_{1-x}Sr_xCoO_{3-\delta}$. That showed a reversible exchange of anion intercalation in the range $0 \leq \delta \leq x/2$resulting in superior pseudocapacitive charge storage in alkaline electrolyte.[176] The $SrRuO_3$ also shows pseudocapacitive charge storage in alkaline media. It was hypothesized that protons migrated along with the lattice oxygen via the Grotthuss mechanism, while redox was attributed to changes in the Ru valence, leading to the formation of $SrRuO_2OH$ resulting in superior charge storage capacity. The researchers also found capacitive behavior for the A- and B-site doped $La_{0.2}Sr_{0.8}Mn_{0.2}Ru_{0.8}O_3$ at 20 mV/s with a mostly rectangular cyclic voltammogram, yielding a maximum capacitance of 160 F/g (53 mAh/g).[177-178]

Figure 1.25 shows O^{2-} intercalation in $SrCoO_{3-\delta}$ for charge storage mechanism in $SrCoO_{3-\delta}$ form ordered perovskite phases with different symmetries in a range between $2.29 < 3-\delta < 3$.[179] Oxygen intercalation was also hypothesized to be the charge storage mechanism in $SrCo_{0.9}Nb_{0.1}O_{3-\delta}$, with the subsequent oxidation of Co^{2+} to Co^{3+} and Co^{4+}. [180]

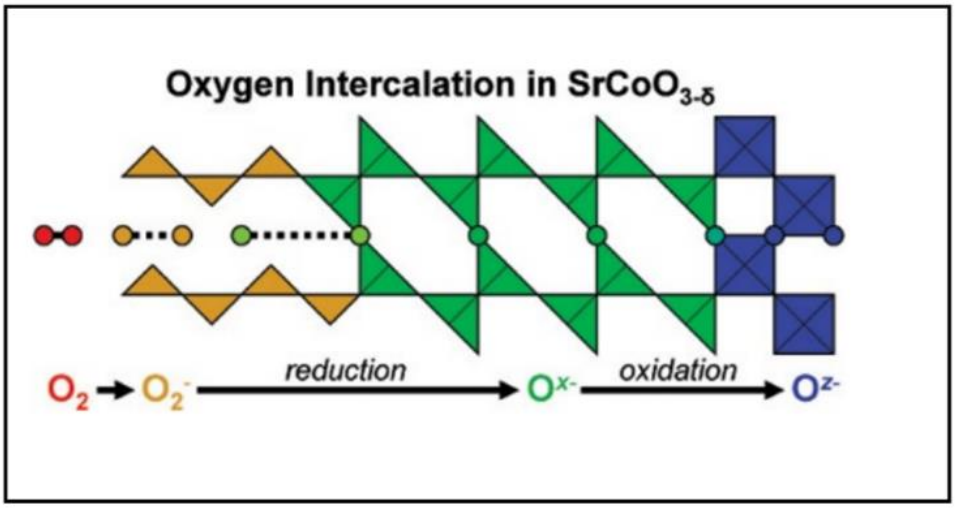

Figure 1.25. shows O^{2-} intercalation in $SrCoO_{3-\delta}$ [179] (Figure is taken from open access internet source)

Assuming the accessible oxygen deficiency/excess range $\delta = 0.25$, the theoretical specific capacity of ca. 110 mAh/g can be calculated for the redox couple $LaMnO_{2.75}/LaMnO_{3.25.}$ The change of oxidation state of the Mn centers was an accumulation of Mn^{4+} found toward the surface of the particles during prolonged cycling due to the addition of oxygen anions from the electrolyte. This was proposed to enhance the diffusion rate of oxygen along the surface and grain boundaries, causing the pseudocapacitive oxygen intercalation kinetics. According to the same mechanism as in $LaMnO_3$, a capacitance of 400 F/g (78 mAh/ g) was reported at 10 mV/s in aqueous KOH, and according to b-value analysis, the process was found to be kinetically surface controlled up to a scan rate of ca. 5 mV/s. Oxygen vacancies in the structure were mainly responsible for pseudocapacitive charge storage in perovskite materials.[181-184]

1.8 Materials showing both OER/ORR catalysis and pseudocapacitance

Materials showing both charge storage and oxygen evolution are very special due to their intrinsic properties. Therefore, such a multifunctional material shows both energy storage and electrocatalytic (OER/ORR) applications are important to study to develop structure-property correlation in developing advanced energy conversion and storage materials

The naturally occurring and abundant transition-metal oxides (TMOs) could be highly successful in this regard as they have high metal ion reactivity and electrochemical stability. [185-187] There are transition-metal oxides that show bifunctional such as charge storage and oxygen evolution such as NiO, [185-186] and Co_3O_4 [187-188] **Figure 1.26** shows the bifunctional charge storage and oxygen evolution behaviour of NiO. RuO_2 also showed excellent OER activity with superior electrochemical stability and high-valued specific capacitance in cooperation with large cycle efficacy**.** [189-190]

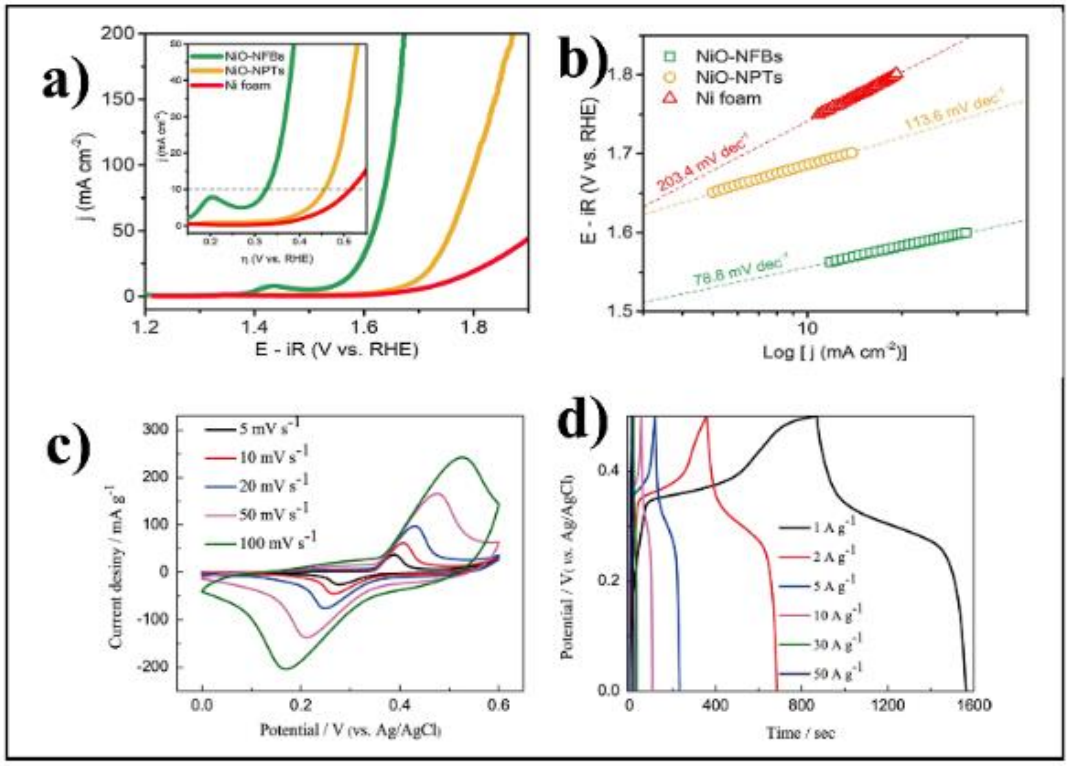

Figure 1.26 a) LSV collected at 5 mV s-1 for NiO-NFBs, NiO-NPTs, and Ni foam electrodes, b) respective Tafel slopes [185] c) CV of NiO nanoparticles film on nickel foams working electrode in 1M KOH d) Galvanostatic charge/discharge profiles for NiO nanoparticles film on nickel in the potential range of 0–0.5V [186] (Figure is taken from open access internet source)

MnO_2 has different crystallographic structures for manganese dioxide, including,α, β, δ, λ,γ, all interlinked by MnO_6 octahedra. **Figure 1.27** (a-d) shows the bifunctional charge storage and oxygen evolution properties of MnO_2. [191-192]

Similarly, several other materials including $NiCo_2O_4$,[193] NiFe double hydroxide,[194] Mn_3O_4,[195-196] FeS_2 ellipsoids,[197] β-$NiMoO_4$,[198] $ZnCo_2O_4$[199] also showed bifunctional charge storage and electrocatalytic OER/ORR activities

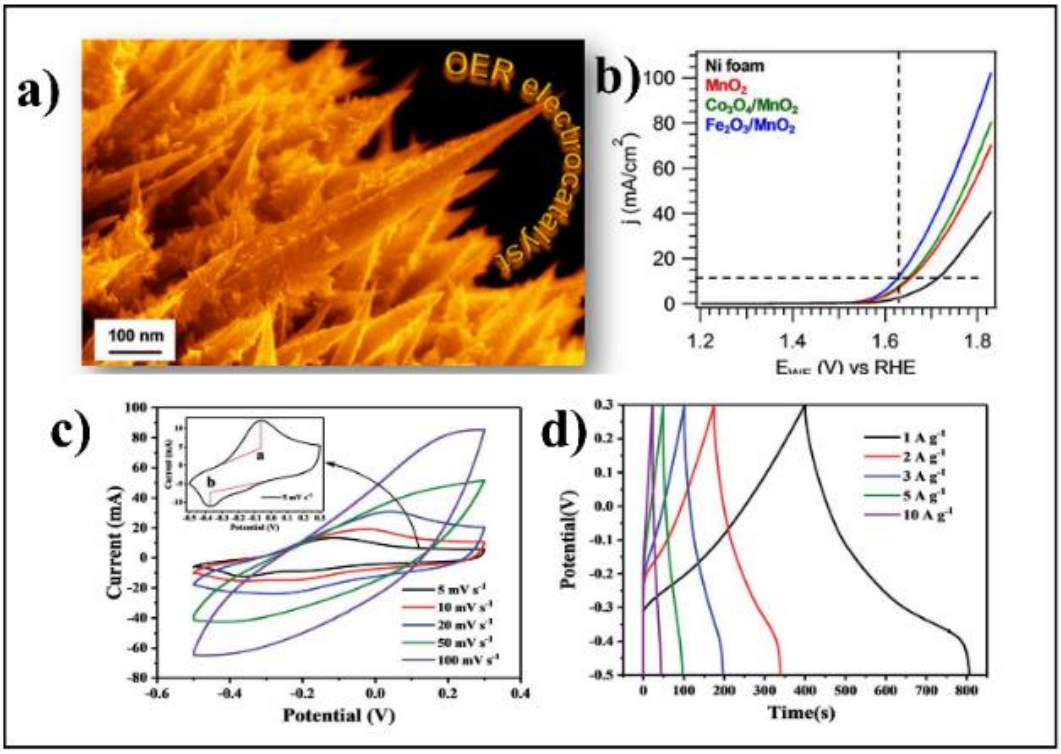

Figure 1.27 a) morphology MnO_2 b) LSV -curves MnO_2-based samples on Ni foam [191]c) CV curves at various scan rates (the inset is the CV curve at 5 mV s-1), d) galvanostatic charge-discharge curves at various current densities of MnO_2 [192] (Figure is taken from open access internet source)

This thesis aims to evaluate and draw a structure-property correlation and develop an understanding of electronic structure correlation to the crystal structure of the materials to develop novel electrocatalysts and pseudocapacitive charge storage materials. We have tried to make a detailed investigation of the charge transfer mechanism and its relation with the host lattice crystal structure resulting in novel pseudocapacitive charge storage and bifunctional OER/ORR activities.